

1

2 **Supplementary Information for**

3 **A biophysical limit for quorum sensing in biofilms**

4 **Avaneesh V. Narla, David Borenstein, and Ned S. Wingreen**

5 **Ned S. Wingreen.**

6 **E-mail: wingreen@princeton.edu**

7 **This PDF file includes:**

- 8 Supplementary text
- 9 Fig. S1
- 10 Tables S1 to S3
- 11 Supplementary references

12 Supporting Information Text

13 Contents

14	S1 Analytical derivation of biophysical limit	2
15	A Autoinduction and metabolic regulation of AI production	3
16	S2 Methods	4
17	A Agent-based modeling	4
18	B Geometry of simulations	4
19	C Initial placement of bacteria	4
20	D Nutrient modeling	4
21	D.1 Reaction-diffusion equation	4
22	D.2 Boundary conditions	4
23	D.3 Influx of nutrient	4
24	E Reproduction and production of matrix	5
25	F Autoinducer	5
26	G AI-dependent reproduction and matrix production	5
27	H Shoving algorithm	5
28	I Pairwise competitions	6
29	S3 Parameters	6
30	S4 Invasion Analysis	6

31 S1. Analytical derivation of biophysical limit

Here we derive the biophysical limit presented in Eq. 2 in the main text. The limit concerns the range of possible autoinducer (AI) concentrations at the surface of bacterial cells. In our model, AI production is proportional to the uptake of a diffusible nutrient (such as O₂). We begin by considering for simplicity a single spherical cell of radius r_0 centered at the origin (our results hold even if the cell is not spherical provided no dimension of the cell is much larger than another). The nutrient diffusion equation, $\frac{\partial c}{\partial t} = D_{O_2} \nabla^2 c$, becomes in steady state,

$$\frac{D_{O_2}}{r^2} \frac{\partial}{\partial r} \left(r^2 \frac{\partial c}{\partial r} \right) = 0,$$

32 where c is the O₂ concentration (representing a generic diffusible nutrient) and D_{O_2} is the diffusion coefficient of O₂ in the
33 medium. Solving this equation with appropriate boundary conditions yields

$$34 \quad c(r) = c_\infty - \frac{r_0}{r} (c_\infty - c_0), \quad r \geq r_0, \quad [S1]$$

35 where we assume a constant O₂ concentration far from the cell, given by $c_\infty = c(\infty)$, and a fixed O₂ concentration, c_0 , at the
36 cell surface. r_0 is the radius of the cell. To find c_0 , we use Fick's Law: the total rate of uptake of O₂ by the cell, J_{O_2} , is

$$37 \quad J_{O_2} = D_{O_2} \oint_S \nabla c = 4\pi D_{O_2} r_0 (c_\infty - c_0), \quad [S2]$$

38 where S is the boundary of the cell.

39 What does this mean for AI production and the distribution of AI around the cell? If we suppose that the cell takes up m
40 molecules of O₂ in the same time that it produces one molecule of AI, the cell's rate of AI production, J_{AI} , is

$$41 \quad J_{AI} = \frac{4\pi D_{O_2} r_0 (c_\infty - c_0)}{m} = -D_{AI} \oint_C \nabla a(\vec{r}), \quad [S3]$$

42 where D_{AI} is the diffusion constant for AI and $a(\vec{r})$ is the concentration of AI outside the cell.

43 Assuming that the cell is the only source of AI, so that the concentration of AI is spherically symmetric and zero far from
44 the cell, and that AI decays at a rate β , we obtain

$$45 \quad a(r) = \frac{D_{O_2}}{m} \frac{(c_\infty - c_0) r_0}{r} \exp\left(-\sqrt{\frac{\beta}{D_{AI}}}(r - r_0)\right) \left(\frac{1}{D_{AI} + \sqrt{\beta D_{AI}} r_0}\right), \quad r \geq r_0. \quad [S4]$$

46 Assuming that the radius of the cell is much smaller than the length-scale of decay of AI concentration ($\sqrt{\frac{D_{AI}}{\beta}}$), we can
47 accurately approximate the AI concentration as:

$$48 \quad a(r) \approx \frac{D_{O_2}}{m D_{AI}} \frac{(c_\infty - c_0) r_0}{r} \exp\left(-\sqrt{\frac{\beta}{D_{AI}}}(r - r_0)\right), \quad r \geq r_0. \quad [S5]$$

49 For $r \gtrsim r_0$, we can further approximate the AI concentration as

$$50 \quad a(r) \approx \frac{D_{O_2}}{mD_{AI}} \frac{(c_\infty - c_0) r_0}{r}, \quad r \geq r_0. \quad [S6]$$

51 Thus, if only one cell is present, the concentration of AI at its boundary is

$$52 \quad a(r_0) \approx \frac{D_{O_2}}{mD_{AI}} (c_\infty - c_0). \quad [S7]$$

53 From Eqs. S1 and S6, we recover an approximate identity between the AI concentration and the O_2 at any point:

$$54 \quad c(r) + \frac{mD_{AI}}{D_{O_2}} a(r) \approx c_\infty, \quad r \gtrsim r_0. \quad [S8]$$

55 This identity becomes exact for all $r > r_0$ in the case $\beta = 0$, when there is no decay of AI.

56 We now extend this result to a system of many cells. As the diffusion equations for AI and O_2 are linear partial differential
57 equations in the concentration, the total distribution of the concentration values in the system is the summation of the
58 distribution of all the cells, centered at the locations of their respective cells. Thus, by using the same boundary conditions for
59 all cells, and for the case of $\beta \rightarrow 0$,

$$60 \quad c(\vec{r}) + \frac{mD_{AI}}{D_{O_2}} a(\vec{r}) \approx c_\infty. \quad [S9]$$

61 Above, we only require that $|\vec{r} - \vec{r}_i| \geq r_0$ where \vec{r}_i is the center of any cell. Thus, the maximum AI concentration for a given
62 set of environmental and physiological parameters is

$$63 \quad \max(a(\vec{r})) = \frac{D_{O_2}}{mD_{AI}} c_\infty, \quad [S10]$$

64 which occurs when $c(\vec{r}) = 0$. We can thus define the dynamic range, DR , as the ratio of this maximum to the minimum AI
65 concentration at the boundary of a cell from Eq. S8:

$$66 \quad DR \equiv \frac{D_{O_2} c_\infty}{mD_{AI}} \frac{mD_{AI}}{D_{O_2} (c_\infty - c_0)} = \frac{c_\infty}{c_\infty - c_0}. \quad [S11]$$

67 What is the dynamic range typically obtained by bacterial cells in a biofilm? Assuming that the intake of O_2 is proportional
68 to the O_2 concentration at the surface of the cell, the flux of O_2 , J_{O_2} , at the boundary of the cell is given by

$$69 \quad J_{O_2} = -c_0 \gamma, \quad [S12]$$

70 where γ is the per-cell rate of intake of O_2 (with units of $1/(\text{concentration} \cdot \text{time})$).

71 Equating Eq. S2 and Eq. S12, we have that

$$72 \quad 4\pi D_{O_2} r_0 (c_\infty - c_0) = c_0 \gamma = (c_\infty - (c_\infty - c_0)) \gamma \quad [S13]$$

$$73 \quad \implies 4\pi D_{O_2} = \left(\frac{c_\infty}{c_\infty - c_0} - 1 \right) \frac{\gamma}{r_0} \quad [S14]$$

$$74 \quad \implies DR \equiv \frac{[AI]_{\max}}{[AI]_{\text{one cell}}} = \frac{c_\infty}{c_\infty - c_0} = \frac{4\pi D_{O_2} r_0}{\gamma} + 1. \quad [S15]$$

77 **A. Autoinduction and metabolic regulation of AI production.** The results above presume that each bacterial cell always consumes
78 m molecules of nutrient for every molecule of AI that it produces, where m has the same value in all conditions. However,
79 bacterial cells may regulate their AI production so as to vary the amount of AI produced per amount of nutrient consumed. In
80 particular, cells may increase the dynamic range of AI concentrations compared to the above limit (Eq. S15) in two ways:
81 either by increasing the rate of AI production per molecule of nutrient when AI concentration is high, or by increasing the
82 rate of AI production per molecule of nutrient when local nutrient availability is low. The former corresponds to the case of
83 autoinduction, where the detection of AI results in activation of AI production, which is commonly observed among many
84 bacterial species that engage in QS (1–3). The latter would require that AI production be prioritized even when nutrient
85 availability is low and includes the case of constitutive AI production (where m would be an inverse function of the limiting
86 nutrient concentration). In either case, AI production is not metabolically slaved, i.e., AI production is not necessarily low
87 when nutrient consumption (and subsequently metabolic activity) is low. Generally, the interior of a biofilm has both a higher
88 AI concentration (due to the higher density of cells) and a lower nutrient concentration than the exterior. Thus, regulation of
89 AI production in either of the forms described above would counteract the lower nutrient concentration in the interior and thus
90 help equalize AI production per cell between the interior and the exterior of the biofilm. The effective AI production rate
91 would then resemble the case of constitutive AI production.

92 S2. Methods

93 **A. Agent-based modeling.** The simulations for this project were performed using Agent-Based Modeling (ABM), a simulation
94 framework that is used widely for academic research in ecology, epidemiology, and the social sciences. It is also used in
95 commercial and governmental uses such as business analytics, supply chain management, and military planning (4).

96 ABM involves representing the system of interest as a collection of autonomous actors (in our case, bacterial cells), which
97 have well-defined behaviors and interact with one another or with the environment (4). The environment itself can be encoded
98 as a set of variables for the simulation. The environment can also evolve with certain dynamics independent of the agents. For
99 example, the environments in our simulations are chemicals such as nutrients used by the bacteria.

100 The benefit of ABM is that global dynamics emerge from many small local interactions. Only local rules are determined
101 and communicated to the program, but one can then study the emergent global interactions.

102 One of the features of ABM is the representation of spatial structure. In our case, spatial structure is important as
103 interactions among bacteria and interactions with the environment are often dictated by the spatial arrangement of cells. For
104 example, one of the attributes we investigate is nutrient availability, where we incorporate a diffusing solute (to model nutrients
105 such as oxygen) into the model. In such a case, spatial structure strongly influences the dynamics of the bacteria such as
106 growth rate. For this project we used an ABM framework known as Nanoverse (4).

107 **B. Geometry of simulations.** The simulations were performed on a square lattice geometry in two dimensions. The shape of
108 the complete simulation domain is a rectangle with a width of 128 squares and a height of 256 squares. Each square in the
109 lattice can either be empty, or be occupied by a bacterial cell, or by matrix. Each square has four neighbors. A zoomed-in
110 region of the simulation domain (of width 7 and height 7) can be seen in Fig. 1A.

111 **C. Initial placement of bacteria.** At the start of each simulated competition, bacterial cells of two different strategies were
112 placed randomly at the bottom of the simulation domain. 64 cells of each strategy were placed randomly in the squares of the
113 bottom row, thus filling the entire bottom row.

114 As a test, we repeated our simulations with reduced numbers of cells at the beginning of the simulation, and found that the
115 results did not vary substantially. Similarly, initially distributing the cells in an alternating ordered pattern did not lead to any
116 substantial differences, and the random distribution was therefore chosen to better reflect natural conditions.

117 D. Nutrient modeling.

118 **D.1. Reaction-diffusion equation.** To obtain steady-state solutions for the diffusive nutrient, we employ a discrete forward-time
119 central-space solver to the reaction-diffusion equation (5). Though this method is valid for all diffusive nutrients with a source
120 far from the biofilm, we refer to the nutrient in our simulations as oxygen (O_2). The bacterial cells are the sinks of O_2 in the
121 reaction-diffusion equation. In general, the concentration of oxygen $[O_2]$ at any site is described by the following differential
122 equation (6):

$$123 \frac{\partial [O_2]}{\partial t} = D_{O_2} \nabla^2 [O_2] - \mu(\vec{x}) [O_2] \delta(\vec{x}), \quad [S16]$$

124 where D_{O_2} is the diffusion constant for O_2 , μ describes the rate of consumption of oxygen, and $\delta(x)$ is a delta function which is
125 nonzero at each bacterial cell. This reaction-diffusion process is solved for the 2D lattice. For simplicity, the discrete grid to
126 solve the equation is taken to be the same as the 2D lattice, i.e., grid spacing equal to the edge-length of a cell. D_{O_2} is taken
127 to be constant everywhere because even at the densest parts of the biofilm, the volume fraction of cells has been experimentally
128 found to be less than 50% (7) and thus the value of D_{O_2} in the entire domain is approximately the value of D_{O_2} observed in
129 water.

130 **D.2. Boundary conditions.** To avoid edge effects, we impose periodic boundary conditions at the horizontal edges of the simulation
131 domain. Thus, a bacterial cell that passes through the right boundary will enter from the left boundary at the same height.
132 Similarly, the concentration of oxygen at the right edge of the simulation domain is the same as the concentration at the left
133 edge at the same height. By imposing this boundary condition, we aim to simulate a large horizontal domain in which the
134 biofilm can grow. Periodic boundary conditions eliminate any exceptional behavior of the biofilm at the horizontal boundaries,
135 as the sites at the boundary are equivalent to any other sites in the domain.

136 **D.3. Influx of nutrient.** A constant, spatially uniform flux of O_2 is introduced to the simulation domain from the top boundary. For
137 a small simulation domain, a source of a limiting diffusible nutrient placed very far away may be approximated by a constant
138 flux boundary condition since the amount of nutrient entering the system will be limited by diffusion and not be impacted by
139 the details of the system (by contrast, a constant value boundary condition on the nutrient leads to a total nutrient flux that
140 can vary with the location of the nutrient-consuming cells). The constant flux boundary condition on O_2 is enforced in our
141 system by designating the top row of the simulation domain as O_2 -producing squares that produce O_2 at a constant rate.

142 O_2 diffuses in the simulation environment from the top boundary towards the bacterial cells. Each bacterial cell consumes
143 O_2 at a rate linearly proportional to the O_2 concentration at its site and acts as a sink of O_2 . Thus, at steady state, the
144 amount of O_2 consumed globally by the cells (δ_{consumed}) is the same as the constant flux of O_2 into the whole system (δ_{in}).
145 The complete simulation domain along with the influx of O_2 represented by arrows (indicating the direction of flux of O_2) can
146 be seen in the snapshot of a simulation in Fig. 1B.

147 **E. Reproduction and production of matrix.** The modeled bacterial cells can perform two actions: reproduction and production
 148 of matrix. Both reproduction and the production of matrix are stochastic processes. At every time step, the probability of a
 149 cell dividing into two cells is calculated from the formula $P(\text{reproduction}) = b_r \cdot [\text{O}_2]\Delta t$, where b_r is the reproduction bias and
 150 Δt is the duration of each time step (if the calculated probability is greater than one, the simulation is immediately halted). A
 151 random real number from a uniform distribution between 0 and 1 is then generated, and if the random number is less than the
 152 probability value for reproduction, the cell produces a copy of itself.

153 Similarly, the probability of matrix production is calculated from the formula $\frac{1}{2}b \cdot [\text{O}_2]\Delta t$ where b is the matrix bias. Every
 154 time step, a random number is generated to decide if *two squares* of matrix will be produced. This algorithm better replicates
 155 the structure of biofilms observed in experiments than an algorithm in which squares of matrix are produced one at a time.
 156 The total biomass production rate per unit of O_2 is constrained such that $\chi b_r + b = 1$ where χ is the cost of reproduction
 157 relative to the cost of producing a square of matrix.

158 The processes of reproduction and matrix production are assumed independent: in the same time step, a cell might reproduce
 159 and also produce two units of matrix. The probability of such a double event occurring is the product of the probabilities
 160 of either event occurring, that is $\frac{1}{2}b b_r [\text{O}_2]^2 (\Delta t)^2$. We chose Δt to be small enough such that the probability of both events
 161 occurring simultaneously is very small ($<0.1\%$).

F. Autoinducer. To incorporate quorum sensing, we introduce autoinducer (AI), the chemical signal produced and sensed by
 bacteria, as a new continuum environmental layer in Nanoverse. The sources of AI are the cells, AI diffuses, and also decays at
 a slow rate.. The boundary conditions for AI are periodic boundary conditions on the left and right boundaries, a reflecting
 (zero-flux) boundary conditions at the bottom boundary, and an absorbing boundary condition at the top boundary. An
 absorbing boundary condition holds the concentration at that boundary to always be 0. Thus the reaction-diffusion equation is
 given by,

$$\frac{\partial[\text{AI}]}{\partial t} = D_{\text{AI}}\nabla^2[\text{AI}] + \delta(\vec{x}) \cdot \Gamma_{\text{AI}}(\text{O}_2) - \beta[\text{AI}],$$

162 with the boundary condition that $[\text{AI}]|_{\text{top boundary}} = 0, \forall t$; D_{AI} is the diffusion constant for AI, $\delta(x)$ is a delta function which
 163 is nonzero at the center of each AI producing cell, Γ_{AI} is the rate of production of AI by that cell, and β is the rate of decay
 164 of AI. We consider two cases: (1) constitutive AI production in which Γ_{AI} is independent of local O_2 concentration, and (2)
 165 nutrient-limited AI production for which Γ_{AI} is proportional to local O_2 concentration.

166 We note that we must assume that AI decays for the geometry of our simulation domain. Since we have an absorbing
 167 boundary condition for the top boundary and total AI production is the same as the total O_2 consumption (which is constant
 168 throughout the simulation), if we don't include decay for AI, we end up with a fixed AI gradient in the region above the cells
 169 (which is equivalent to the case of a fixed flux of AI leaving the cells). Thus, when the cells line the bottom of the domain,
 170 local AI is maximal, and as the layer of actively-growing cells moves up the simulation domain, the local AI at those cells drops
 171 steadily. We include decay for AI to avoid this scenario.

172 **G. AI-dependent reproduction and matrix production.** In the model, The reproduction bias, b_r , and the matrix production bias,
 173 b , may depend on the local AI concentration. Specifically, b is then given by the following expression:

$$b([\text{AI}]) = b_{\min} + (b_{\max} - b_{\min}) \frac{[\text{AI}]^h}{K^h + [\text{AI}]^h}. \quad [\text{S17}]$$

174 The terms in S17 are as follows:

- 175 1. b_{\min} is the minimum possible value of b ;
- 176 2. b_{\max} is the maximum possible value of b ;
- 177 3. K is the AI concentration at which b attains the value $\frac{1}{2}(b^{\min} + b^{\max})$;
- 178 4. h is the Hill coefficient, which characterizes cooperativity.

179 The matrix production bias, b , is still related to b_r by the equation:

$$\chi b_r([\text{AI}]) + b([\text{AI}]) = 1.$$

180 These forms for b and b_r reflect the relatively switch-like behavior exhibited by many quorum-sensing bacteria. The behavior is
 181 more switch-like for higher values of h .

182 **H. Shoving algorithm.** Our simulation does not incorporate cell death, and no cells or matrix are removed from the simulation.
 183 With matrix production and reproduction, the volume of biomass strictly increases and new lattice sites become occupied. As
 184 the cells that reproduce or produce matrix may be in the interior of the biofilm, these cells must shove biomass towards the
 185 edge of the biofilm to make room for new cells/matrix. The algorithm for shoving is detailed below and the cumulative result
 186 of all steps is depicted in Figs. 1B and 1C. Steps 1-5 are common for both matrix production and reproduction. All distances
 187 are measured by L_1 distance, also known as Manhattan distance.

- 188 1. The closest vacant sites to the parent site (the site reproducing or producing matrix) are identified.

- 189 2. One of the closest vacant sites is chosen randomly.
- 190 3. The shortest paths to the chosen vacant site are identified. Paths are sequences of distinct lattice sites. All lattice sites in
191 a path must be cardinal neighbors (N, S, E, or W) to the lattice sites before or after them in the path. The last lattice
192 site in the path to a vacant site is the vacant site itself.
- 193 4. One of the shortest paths is chosen randomly.
- 194 5. All of the occupants of the lattice sites in the path are “shoved” to occupy the next lattice site in the path. Thus, the
195 second lattice site of the path, after the active site, is now empty. This lattice site will be called the daughter site.
- 196 6. If the action is reproduction, a copy of the reproducing cell is placed in the daughter site (Fig. 1B).
- 197 7. If the action is matrix production, half of the time the matrix will occupy the daughter site (and the cell will occupy the
198 matrix site). The other half of the time, the cell will occupy the daughter site, and the matrix will occupy the parent site.
199 The choice between these two alternatives is made randomly.

200 The algorithm for shoving is extremely important as spatial structure is a crucial feature of biofilm growth. Our algorithm
201 results in a compact biofilm as observed in nature (because the nearest vacant sites are occupied first). It also causes a
202 homogeneous distribution of matrix and bacterial cells because the cells are pushed away from the parent site and towards the
203 edge of the biofilm only half of the time. The other half of the time, the cells stay at the parent site.

204 For the bacteria and the matrix, the bottom boundary acts as a hard boundary. Thus, neither bacteria nor matrix can be
205 shoved past the bottom of the simulation domain.

206 **I. Pairwise competitions.** In this investigation, we compare bacteria with different matrix production strategies and assess the
207 competitive advantage that each strategy affords in a nutrient-limited environment. To evaluate the competitive advantage of
208 strategies, we performed pairwise competitions between bacteria of different strategies. As noted above, we started simulations
209 with an equal number of cells of each strategy, placed randomly along the bottom row of the simulation domain. We then
210 allowed the simulation to run until either of three specified halt conditions occurred. The first halt condition was an occupancy
211 of 50% of the sites (that is, if 50% of the sites were filled with matrix or with bacterial cells of either strategy, the simulation
212 would stop). The other halt conditions were any one bacterial cell reaching the top boundary of the simulation domain or the
213 probability of either reproduction or matrix production by a bacterial cell being greater than unity.

214 To evaluate the competitive advantage of the strategies, we recorded the number of cells of each strategy at the end of the
215 simulation.

216 S3. Parameters

217 There are two relevant timescales in our simulations: the timescale of biomass production (both through reproduction and
218 matrix production), and the timescale for the reaction-diffusion processes to equilibrate. We assume that there is a separation
219 of timescales, as the former (typically on the order of 30-60 minutes) is much much longer than the latter (on the order of 20
220 seconds for a region of the size we consider). In practice, this means that we calculate the steady-state O_2 and AI concentrations
221 for each fixed arrangement of cells and matrix, and then update the latter. The parameters for the reaction-diffusion equations
222 are given in Table S1. The value of the flux of O_2 entering the system is essentially arbitrary, since the steady-state O_2
223 concentration simply scales with this flux, and the O_2 concentration is absorbed into an arbitrary linear relation between O_2
224 consumption and biomass production. Each lattice site in the domain is taken to be $1 \mu\text{m}$ by $1 \mu\text{m}$, and this sets the length
225 scale for the reaction-diffusion equations at $1 \mu\text{m}$. We take the timescale for reaction-diffusion to be 1s. The diffusion constant
226 for O_2 is taken to be $2000 \mu\text{m}^2/\text{s}$, the value for O_2 diffusion in water at 20C at ambient pressure (8). For these parameters,
227 the penetration depth of O_2 for maximally dense simulated cells is $0.3 \mu\text{m}$. The parameters used to generate the results for
228 quorum-sensing cells are described in Table S2.

229 S4. Invasion Analysis

230 In principle, a particular matrix-production strategy might have a competitive advantage in a 1:1 competition with another,
231 and yet lose that advantage when it initially constitutes a different fraction of the population. This would be an example
232 of frequency-dependent selection. To investigate this possibility in a representative case, we performed simulations of a QS
233 strategy versus a fixed strategy as shown in Fig. S1. We find that the constitutive QS strategy preserves its large competitive
234 advantage when it is initially much more common than a competing fixed strategy down to when it is a few-fold lower than a
235 competing fixed strategy. However, at very low initial fractions, the QS strategy has only a modest competitive advantage.
236 This is because without the minimal number of cells to produce sufficient AI, the QS cells fail to switch from their initial high
237 matrix bias to a low matrix bias that would allow them to capitalize on achieving a local monopoly on access to the diffusive
238 nutrient.

239
240

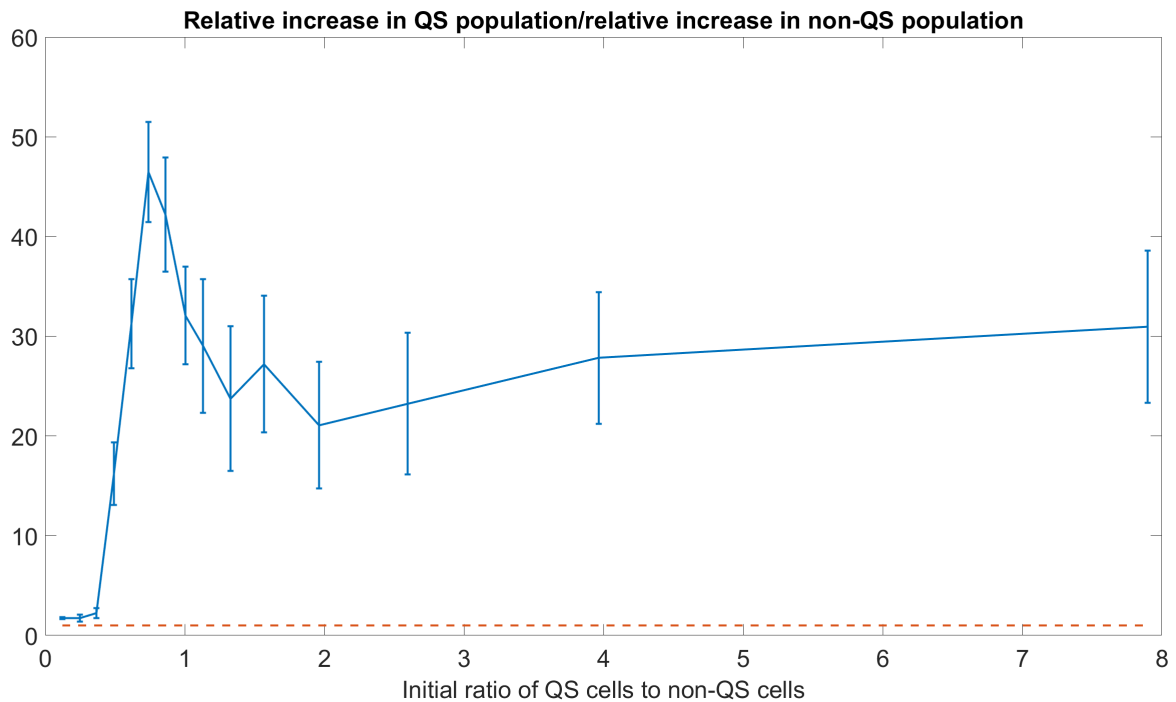


Fig. S1. Ratio of the increase in population of the QS strain to the increase in population of the fixed strategy strain (with a matrix bias of 0.3) for different ratios of the starting populations. The reference red line indicates ratio 1, i.e. equal performance of the two strains.

Property	Value (in dimensionless units)
Total flux of O ₂ entering the system	128×10^{-5}
O ₂ diffusion constant	2000
O ₂ consumption rate per bacterial cell	2×10^4
Cost of reproduction relative to matrix production (for equal volumes)	14 (9)

Table S1. Non-dimensionalized parameters for the reaction-diffusion equations based on units of μm and seconds.

References

1. BL Bassler, R Losick, Bacterially speaking. *Cell* **125**, 237–246 (2006).
2. ST Rutherford, BL Bassler, Bacterial quorum sensing: its role in virulence and possibilities for its control. *Cold Spring Harb. Perspectives Medicine* **2**, a012427 (2012).
3. W Haas, BD Shepard, MS Gilmore, Two-component regulator of enterococcus faecalis cytolysin responds to quorum-sensing autoinduction. *Nature* **415**, 84–87 (2002).
4. DB Borenstein, A multi-agent approach to the evolution of microbial populations in the presence of spatially structured social interaction, Ph.D. thesis (Princeton University) (2015).
5. PJ Roache, *Fundamentals of Computational Fluid Dynamics*. (Hermosa Publishers), (1998).
6. DB Borenstein, Y Meir, JW Shaevitz, NS Wingreen, Non-local interaction via diffusible resource prevents coexistence of cooperators and cheaters in a lattice model. *PLOS ONE* **8**, e63304 (2013).
7. K Drescher et al., Architectural transitions in *Vibrio cholerae* biofilms at single-cell resolution. *Proc. Natl. Acad. Sci.* **113**, E2066–E2072 (2016).
8. RB Bird, WE Stewart, EN Lightfoot, *Transport Phenomena*. (John Wiley & Sons) Vol. 413, (1960).
9. J Yan, CD Nadell, BL Bassler, Environmental fluctuation governs selection for plasticity in biofilm production. *The ISME J.* **11**, 1569–1577 (2017).

Property	Description	Value
h	Coefficient of cooperativity	10
b^{\min}	Minimum value of matrix bias obtained	0.1
b^{\max}	Maximum value of matrix bias obtained	0.9
K	AI concentration at which b attains the value $\frac{1}{2}(b^{\min} + b^{\max})$	0.5
Γ_{AI}	AI production rate for constitutive AI producers	10^{-7}
D_{AI}	Diffusion constant of AI	160
β	AI decay rate	10^{-4}

Table S2. Parameters used to incorporate QS bacteria into the simulations in units of μm and seconds.

Property	Description	Value
h	Coefficient of cooperativity	10
b^{\min}	Minimum value of matrix bias obtained	0.1
b^{\max}	Maximum value of matrix bias obtained	0.9
K	AI concentration at which b attains the value $\frac{1}{2}(b^{\min} + b^{\max})$	3.5
Γ_{AI}	AI production rate per unit concentration of oxygen per cell	10^{-4}
D_{AI}	Diffusion constant of AI	160
β	AI decay rate	10^{-2}

Table S3. Parameters used to incorporate QS bacteria that produce AI at a rate proportional to O_2 uptake in units of μm and seconds.